International Journal of Engineering Science and Advanced Technology (IJESAT)
Vol 26 Issue 05, May 2026
Received: 19-03-2026 Accepted: 25-04-2026 Published: 02-05-2026

EXPERIMENTAL PERFORMANCE ASSESSMENT OF AN INTERNALLY-COOLED MINI-CHANNEL FINNED-TUBE HEAT EXCHANGER AS A LIQUID DESICCANT–AIR CONTACTING DEVICE IN A HYBRID AIR-CONDITIONING SYSTEM

Shemal Parmar[1], Jagdish Talpada[2], Chetan Somani[3], Manish Prajapati[4]
Department of Mechanical Engineering, Polytechnic college
The Maharaja Sayajirao University of Baroda, Vadodara, Gujarat, India, shemalparmar-polymed@msubaroda.ac.in

Abstract*—Compact heat exchangers employing mini-channel flow passages, with hydraulic diameters in the range of 0.2–3 mm, provide elevated surface-area-to-volume ratios, enhanced heat-transfer coefficients and reduced refrigerant inventories compared with conventional finned-tube coils. The present work investigates the suitability of a finned-tube mini-channel coil as the internally-cooled air–liquid-desiccant (LD) contacting device of a hybrid liquid desiccant air-conditioning (LDAC) unit. An instrumented experimental facility integrating a vapour-compression chiller, a centrifugal-pump-driven LD spraying loop and an acrylic-enclosed coil was constructed and tested under two modes—chilled-water-only and chilled-water with sprayed aqueous LD—at coil-inlet chilled-water temperatures of 17 °C and 22 °C. The water, air and desiccant mass flow rates were maintained at 200 L/h, 0.155 kg/s and 86.71 kg/h, respectively. A peak total cooling rate of 2.5 kW was obtained with chilled water alone at 17 °C, whereas the introduction of the LD spray raised sensible cooling marginally (from 1.4 to 1.6 kW at 17 °C) but reduced latent cooling from 1.1 kW to 0.3 kW and total cooling from 2.5 kW to 1.9 kW. The performance penalty is attributed to the additional air-side thermal resistance imposed by the desiccant film and to the short gas–liquid contact time at the prevailing face velocity. The results delineate the operating regime in which mini-channel coils can function effectively as internally-cooled LD contactors and identify the LD-to-air mass-flow ratio and desiccant pre-cooling as the dominant levers for further improvement.*

***Index Terms*—**Hybrid liquid desiccant air conditioning, mini-channel heat exchanger, internally-cooled dehumidifier, finned-tube coil, dehumidification effectiveness, moisture removal rate, hybrid HVAC.

I. INTRODUCTION

Thermal comfort conditioning of built spaces is one of the largest end-uses of electricity in both residential and commercial sectors, and the proportion of that demand associated with latent-load handling has been steadily growing as building envelopes become tighter and outdoor ventilation-air enthalpies rise in humid climates [1], [2]. Conventional vapour-compression refrigeration (VCR) systems address humidity by overcooling the supply air below its dew point so that moisture condenses on the cooling coil. This approach couples sensible and latent cooling, forces reheat energy penalties when space sensible loads are low, produces a permanently wet surface that favours microbial activity, and ties moisture control to the electrical compressor, which limits efficiency at part load [3], [4].

Liquid desiccant (LD) technology has re-emerged as a robust alternative because it decouples latent from sensible handling. A hygroscopic aqueous salt solution—most commonly lithium chloride (LiCl), calcium chloride ($CaCl_2$) or a mixture thereof—placed in direct or membrane-separated contact with process air absorbs water vapour at temperatures well above the air dew point, enabling cold-water loops to be operated at higher temperatures, reducing the sensible heat ratio that the chiller must deliver and permitting regeneration of the diluted desiccant from low-grade heat sources such as solar collectors, waste heat or condenser rejection [5]–[7]. Recent reviews confirm that hybrid LDAC–VCR configurations routinely achieve 20–30 % primary-energy savings compared with stand-alone VCR under high latent-load operation, while simultaneously improving indoor air quality by scrubbing airborne pollutants through the desiccant film [8]–[10].

The bottleneck of every LD system is the air–solution contactor. In an adiabatic dehumidifier the desiccant temperature rises continuously as it absorbs moisture, which progressively raises its equilibrium vapour pressure and chokes the driving potential for mass transfer. Internal cooling—where a chilled-water loop removes the heat of absorption and the sensible component simultaneously—sustains a large driving potential along the full length of the contactor and significantly improves the dehumidification effectiveness [11], [12]. Several contactor architectures have been proposed, including packed beds, spray towers, falling-film fin-tube coils, plate exchangers with alternating air and desiccant channels, hollow-fibre membrane modules and bubble columns [13]–[16]. Each configuration trades off between surface wetting, film stability, carry-over of desiccant droplets into the air stream, and volumetric compactness.

In parallel, developments in compact heat-exchanger technology have produced mini-channel coils with hydraulic diameters (D_h) in the range 0.2–3 mm, in which the Nusselt

International Journal of Engineering Science and Advanced Technology (IJESAT)
Vol 26 Issue 05, May 2026
Received: 19-03-2026 Accepted: 25-04-2026 Published: 02-05-2026

number, pressure-drop behaviour and two-phase flow regimes depart markedly from conventional channels [17]–[19]. Mini-channel coils have delivered 7–12 % higher cooling capacities in automotive air-conditioning evaporators compared with geometrically identical laminated types [20], and have enabled refrigerant-charge reductions in the 15–25 % range [21]. Their very high surface-area-to-volume ratios, aluminium construction and low coolant hold-up also make them attractive candidates as the process-air side of an internally-cooled LD contactor, particularly when aqueous (non-corrosive) coolants are used and the desiccant is kept off the inner surface.

Nevertheless, the published literature on mini-channel coils as LD–air contacting devices is still sparse. Most internally-cooled experimental studies have employed plate exchangers or finned bundles with conventional tube diameters [22], [23]; those addressing mini- or micro-channel geometries are focused on single-phase water- or refrigerant-side performance, leaving open the question of whether the intrinsic compactness advantage of mini-channels is preserved when a desiccant film coats the external surface and introduces an additional mass- and heat-transfer resistance [24].

The present work addresses this gap. A vertical finned-tube mini-channel coil served by a dedicated VCR chiller was instrumented and tested in two modes—chilled-water-only (baseline) and chilled-water with externally sprayed aqueous LiCl desiccant—at two chilled-water inlet temperatures (17 °C and 22 °C) representing values above and close to the air dew-point. The specific objectives were: (i) to quantify the sensible, latent and total cooling delivered by the coil in each operating mode; (ii) to isolate the marginal contribution (or penalty) associated with the introduction of the LD film; (iii) to evaluate the dehumidification effectiveness and moisture removal rate (MRR) of the integrated contactor; and (iv) to identify the dominant parameters governing the hybrid-system performance envelope.

The remainder of the paper is organised as follows. Section II reviews recent progress in mini-channel heat exchangers, liquid desiccant materials, internally-cooled contactor architectures and hybrid LDAC systems. Section III describes the experimental setup and measurement protocol. Section IV presents the governing equations used to reduce the experimental observations. Section V discusses the measured performance and contrasts the two operating modes. Section VI summarises the main conclusions and outlines the scope for future work.

II. LITERATURE REVIEW

A. Mini-channel heat exchangers

Kandlikar's widely cited channel classification places hydraulic diameters of 3 mm > D_h > 0.2 mm in the mini-channel regime and diameters below 0.2 mm in the micro-channel regime, with distinct flow physics in each [17]. Tran and Wang [19] optimised the air-side performance of flat-tube mini-channel radiators using composite straight-and-louvered fins and reported heat-transfer coefficients 15–22 % higher than those of plain-fin baselines at equal pumping power. Wang et al. [25] experimentally characterised laminar-flow heat transfer in a harmonica tube with mini-fins and observed a Nusselt-number enhancement of 30–45 % relative to the smooth reference geometry. Vangeffelen et al. [26] derived a periodically-developed Nusselt-number correlation for offset-strip fins in mini- and micro-channels that closes the gap between fully-developed assumptions and the periodic thermal boundary layers that develop behind the fin breaks.

Two-phase studies are equally abundant. Wen et al. [27] investigated flow boiling in serrated-fin mini-channels and proposed a correlation valid from 200 to 1500 kg m^{-2} s^{-1} that captures 94 % of the data within ±25 %. Li et al. [28] measured the frictional pressure drop of R134a in mini-channels with micro pin-fins during flow boiling and showed that the pin-fin geometry lowered the two-phase frictional multiplier by up to 28 % compared with plain mini-channels. Vaisi et al. [29] experimentally compared wavy and strip fins in multi-fluid compact condensers and found that strip fins delivered 12 % higher condensation heat-transfer coefficients at the cost of a 9 % pressure-drop penalty. Chang and Chen [30] reported that spirally finned tube bundles subjected to pitching and rolling motions—representative of marine applications—exhibit hydrothermal enhancements of 10–16 % over static operation owing to secondary-flow intensification.

Data-driven approaches are also being applied. Zhu et al. [31] used gradient-boosted decision trees to predict flow-boiling and condensation heat-transfer coefficients in serrated-fin mini-channels, obtaining mean absolute errors below 8 % across the complete working range. Wen et al. [32] coupled experiments with an artificial neural network to describe the performance of ZnO–ethylene-glycol/water nanofluids in mini-channels with serrated fins, highlighting the potential of composite fin geometries to counteract the viscosity penalty that accompanies nanoparticle loading. Thermal-property measurements of water/ZnO nanofluids in offset-fin mini-channels by Wen et al. [33] further confirmed that nanofluids can raise the convective coefficient while leaving the pressure-drop correlation structurally unchanged.

Geometry-optimisation efforts include Ozturk et al. [34], who investigated offset-strip fins with non-uniform uninterrupted fin length and obtained a 6 % improvement in the j/f ratio, and Bahiraei and Monavari [35], who analysed the irreversibility characteristics of a mini-shell-and-tube exchanger operating with boehmite-alumina nanofluid and reported that platelet-shape nanoparticles with fins minimise entropy generation. Venegas et al. [36] proposed a new mini square-channel air-cooled heat exchanger for absorption chillers with a footprint 35 % smaller than the conventional solution at equal UA.

2250-3676 ijesatj@gmail.com https://www.ijesat.com/

International Journal of Engineering Science and Advanced Technology (IJESAT)
Vol 26 Issue 05, May 2026
Received: 19-03-2026 Accepted: 25-04-2026 Published: 02-05-2026

B. Liquid desiccant materials and fundamentals

LiCl and $CaCl_2$ remain the workhorse desiccants for building applications because of their large water-vapour pressure depression per unit cost and their compatibility with polymer-lined components. Bai et al. [37] showed that mixing LiCl and $CaCl_2$ at an optimum mole ratio of 1:2 in a membrane-based dehumidifier reduced the total cost by 18 % while retaining 93 % of the pure-LiCl dehumidification effectiveness. Das et al. [38] quantified the performance of falling-film LiCl and $CaCl_2$ dehumidifiers with surface modifications and reported that hydrophilic coatings raised the wetted area fraction from 0.72 to 0.94, translating into a 21 % increase in moisture removal rate. Ijas Ahmed and Gangadhara Kiran Kumar [39] measured $CaCl_2$-based dehumidification under tropical humid conditions and showed that latent loads up to 2.6 kW could be handled by a compact falling-film column at inlet humidities of 19 g/kg.

Ionic liquids (ILs) have been proposed as next-generation desiccants owing to their negligible vapour pressure and adjustable affinity for water. Bai et al. [40] reviewed recent progress in IL-based dehumidification and concluded that 1-ethyl-3-methylimidazolium acetate and related cations can reduce regeneration temperatures by 15–20 K relative to LiCl at matched saturation humidity, albeit at significantly higher first cost. Wei et al. [41] examined the heat-transfer characteristics of CO_2 refrigerant coupled with $CaCl_2$ aqueous solution in a combined gas cooler/evaporator and suggested synergies for trans-critical heat pumps with LD dehumidification.

C. Internally-cooled LD contactors

Guan et al. [42] provided a comprehensive review of internally-cooled LD air dehumidifiers covering materials, components, systems and performances, and highlighted that internal cooling raises the dehumidification effectiveness by 25–40 % relative to adiabatic counterparts at matched contactor surface area. Naveen and Kolakoti [43] systematically catalogued internal-cooling strategies—plate-fin, finned-tube, membrane, hollow-fibre and bubble-column—and proposed a normalised comparison metric (moisture removal per unit exchanger volume per unit pump+fan power) that favours internally-cooled finned-tube geometries for air flow rates below 0.5 kg/s. Luo et al. [44] quantitatively contrasted adiabatic and internally-cooled processes with a validated numerical model and showed that internal cooling sustains the driving vapour-pressure difference at 50–70 % of its inlet value along the length of the contactor, compared with only 20–30 % in the adiabatic case.

Zhang et al. [45] developed a counter-crossflow indirect evaporative cooling-assisted LD dehumidifier and demonstrated a dehumidification effectiveness of 0.72 at an inlet humidity of 18 g/kg and an air-to-desiccant mass ratio of 3. Zhang et al. [46] applied response-surface modelling to an internally-cooled LDAC system and identified chilled-water temperature, desiccant concentration and air face velocity as the three dominant parameters, accounting for 87 % of the variance in the moisture-removal rate. Li and Yao [47] compared counter-flow, parallel-flow and cross-flow arrangements in internally-cooled membrane-based LD dehumidifiers and reported that counter-flow achieved the highest dehumidification effectiveness (0.81) but required the tightest membrane pressure-balance tolerances.

Zhang et al. [48] formulated a 4-NTU–Le heat- and mass-transfer model for a novel microchannel flat-tube/rectangular corrugated-fin internally-cooled LD dehumidifier and validated it against experiments; the model predicted moisture removal within ±7 % across 96 test points. Wang et al. [49] experimentally analysed a hollow-fibre membrane dehumidifier with a $SiO_2/CaCl_2$ desiccant solution and showed that the nano-silica additive raised the convective mass-transfer coefficient by 14 % through a combination of Brownian motion and enhanced film wetting. Indrawan et al. [50] studied dehumidification and regeneration in a fin-and-tube LD system and reported a coupled COP of 0.68 at a regeneration temperature of 65 °C. Shah et al. [51] investigated a novel bubble-column LD dehumidifier with internal cooling and obtained a dehumidification effectiveness of 0.78 with a compact 0.45 m tall column, confirming the penetration-theory limits.

From the mini-channel side, Pasqualin and Davies [52] proposed a multi-stage nanofiltration concept for LD regeneration in greenhouse cooling and later reported dynamic simulations of a novel LD air-conditioning unit coupled to water recovery [53]. Park et al. [54] applied an LD-assisted free-cooling approach to hot-and-humid-climate data centres and achieved a 24 % annual primary-energy saving relative to the baseline DX system. Allahham et al. [55] demonstrated that integration of chimney ventilation, LD dehumidification and indirect evaporative cooling can cover over 80 % of the thermal-comfort hours in tropical climates without mechanical cooling. Huang et al. [56], [57] showed that combining surfactant additives and internal cooling in LD dehumidifiers enhances volatile-organic-compound (VOC) transfer, extending the role of the LD system from humidity control to broader indoor-air-quality management.

D. Hybrid LDAC-VCR systems

Kumar et al. [58] reviewed the progressive development of hybrid LD–vapour-compression cooling systems and classified existing architectures according to where the desiccant loop is inserted relative to the evaporator. Chen et al. [59] provided an earlier comprehensive review on LD dehumidification and air-conditioning systems, noting that independent temperature and humidity control affords COP improvements in the range 1.2–1.8 compared with standard VCR at identical comfort conditions. Zhang et al. [60] proposed an ideal mass-transfer cycle as a thermodynamic target for LDAC design and showed that real systems operate at 40–60 % of the ideal limit, leaving substantial scope for optimisation. Shukla and Modi [61] reviewed the influence of

International Journal of Engineering Science and Advanced Technology (IJESAT)
Vol 26 Issue 05, May 2026
Received: 19-03-2026 Accepted: 25-04-2026 Published: 02-05-2026

distinct input parameters—air inlet humidity, desiccant concentration, air-to-solution flow ratio and chiller supply temperature—on dehumidifier, regenerator and coupled LDAC evaporative-cooling performance. Qu et al. [62] reported a validated model of an optimised hollow-fibre LDAC system for Mediterranean climates, achieving a 31 % reduction in annual HVAC electricity consumption.

Khosravi et al. [63] compared direct and desiccant-assisted evaporative cooling using novel candidate materials and highlighted the importance of dew-point approach in climates with moderate wet-bulb temperatures. Fang et al. [64] introduced a cascade deep-dehumidification concept combining direct-contact cooling with LD absorption to reach supply dew points below 5 °C, relevant for pharmaceutical and electronics cleanrooms.

E. Research gap and positioning

The collected body of work confirms that (i) mini-channel compact coils outperform conventional coils in single-phase and two-phase thermal-hydraulic terms, (ii) internal cooling is mandatory for high-effectiveness LD dehumidification, and (iii) hybrid LDAC–VCR systems can reduce primary-energy demand in latent-load-dominant buildings. However, experimental evidence on the use of a finned-tube mini-channel coil simultaneously as the evaporator of a VCR chiller and as the internally-cooled contacting surface of an LD sprayer is limited. The present study therefore instruments such a coil and measures its sensible, latent and total cooling delivery under coupled operation, providing the first side-by-side data set that quantifies the penalty or benefit associated with LD introduction onto a compact mini-channel surface at two chilled-water temperatures representative of above- and near-dew-point operation.

III. EXPERIMENTAL SETUP AND METHODOLOGY

A. System description

The experimental facility, shown schematically in Fig. 1 and photographed in Fig. 2, was assembled at the Department of Mechanical Engineering, The Maharaja Sayajirao University of Baroda. It comprises the following principal sub-systems: (i) a vertically oriented finned-tube mini-channel heat exchanger that serves simultaneously as the VCR evaporator and as the internally-cooled contacting surface; (ii) a VCR chiller delivering chilled water to the coil; (iii) a liquid-desiccant recirculation loop composed of an aqueous LiCl reservoir, a centrifugal pump and a spray-distribution header positioned above the coil; (iv) a cellulose evaporative pad upstream of the coil to stabilise air humidity excursions; (v) a centrifugal blower that draws ambient air through the test section at a constant face velocity; and (vi) an acrylic enclosure of 4 mm wall thickness that provides visual access to the coil surface while minimising stray infiltration. The system layout and the principal flows are indicated in Fig. 3.

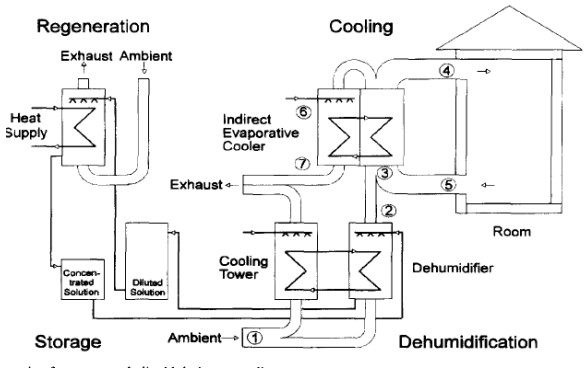

Fig. 1. Open-cycle LDAC cooling configuration combining a regeneration loop, storage of concentrated/diluted solution and a dehumidification–cooling circuit served by an indirect evaporative cooler.

The process-air path is as follows. Ambient air, drawn through the cellulose pad, enters the acrylic enclosure and encounters the finned-tube mini-channel coil. In coil-only operation the coil is internally cooled by the chilled-water loop, producing sensible cooling and, when the surface temperature is below the local air dew point, partial condensation. In LD-integrated operation, aqueous LiCl is sprayed from the top header onto the fin surfaces; gravity drives the film downward in a falling-film arrangement while the air flows vertically upward through the gaps. The diluted desiccant is collected at the bottom sump and recirculated through the pump.

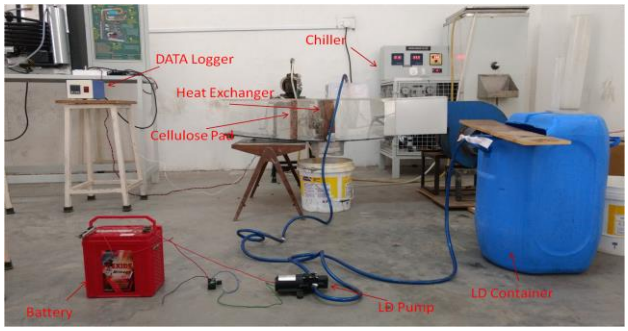

Fig. 2. Photograph of the experimental facility showing the VCR chiller, the data logger, the cellulose evaporative pad, the mini-channel heat exchanger on its stand, the LD container, the LD pump and the battery supply for the ancillary instrumentation.

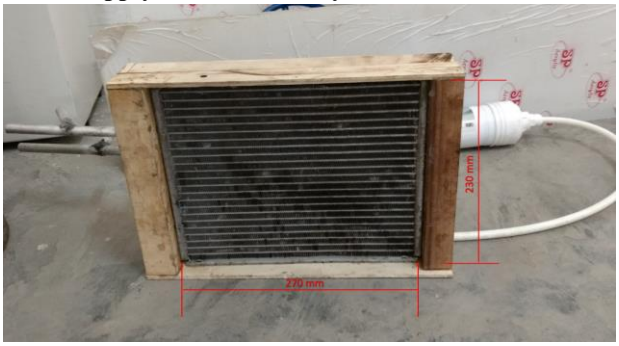

Fig. 3. Close-up view of the vertical finned-tube mini-channel coil used as the internally-cooled contacting device.

International Journal of Engineering Science and Advanced Technology (IJESAT)
Vol 26 Issue 05, May 2026
Received: 19-03-2026 Accepted: 25-04-2026 Published: 02-05-2026

B. Operating parameters

All the tests reported in this paper were performed at the following nominal conditions, held constant to ensure inter-test comparability: water mass flow rate = 200 L/h, air mass flow rate = 0.155 kg/s (equivalent to a fan-delivered volumetric flow of 0.126 m³/s after accounting for local density), and LD mass flow rate = 86.71 kg/h whenever the desiccant loop was engaged. The two chilled-water inlet temperatures investigated were T_w = 17 °C (below the ambient air dew point) and T_w = 22 °C (above the ambient air dew point). The ambient temperature and relative humidity were monitored continuously to confirm a quasi-steady environment; all measurements reported below correspond to a dry-bulb range of 33.5–35.7 °C and a relative humidity range of 36.4–45.5 %, which correspond to the March climate of Vadodara.

C. Instrumentation

Air dry-bulb temperature and relative humidity at the coil inlet and outlet were measured with HTC Easy-Log data loggers (range −20 °C to 199.9 °C, accuracy ±(3 % of reading + 4 °C) for temperature; 5–98 % RH, ±3.5 % RH for humidity). Air velocity was recorded with a vane anemometer over the range 0.1–15 m/s, accuracy ±(0.1 m/s + 2 % of reading). Chilled-water temperatures at the coil inlet and outlet and the LD bulk temperature were measured with type-K thermocouples with an accuracy of ±0.5 °C. The instrument specifications are summarised in Table I.

TABLE I
MEASURING INSTRUMENTS AND SPECIFICATIONS

Sr. No.	Property Measured	Instrument	Range	Accuracy
1	Air velocity	Vane anemometer	0.1–15 m/s; 0–60 °C	±(0.1 m/s + 2 %); ±0.5 °C
2	Air dry-bulb temperature	HTC Easy Log	−20 to +199.9 °C	±(3 % rdg + 4 °C)
3	Air relative humidity	HTC Easy Log	5 to 98 % RH	±3.5 % RH
4	Water / LD temperature	Type-K thermocouple	0–200 °C	±0.5 °C

D. Test protocol

Two back-to-back test blocks were executed under the same ambient conditions to minimise the influence of environmental drift on the cross-comparison. In the first block, chilled water was circulated through the coil at 200 L/h while no desiccant was sprayed; inlet and outlet air temperature and humidity, inlet and outlet chilled-water temperature, and air face velocity were recorded at 60 s intervals for 25 min after thermal stabilisation. In the second block, performed immediately after the first at the same water temperature and flow rate, the LD pump was activated to deliver 86.71 kg/h of aqueous LiCl onto the coil, and the same instruments were sampled for 25 min. Each block was repeated at T_w = 17 °C and at T_w = 22 °C, yielding the four characteristic operating points reported in Section V.

IV. MATHEMATICAL FORMULATION

The observations were reduced to sensible, latent and total cooling rates, dehumidification effectiveness and moisture removal rate using the ASHRAE moist-air property framework [9], [61]. The saturation vapour pressure of water vapour at dry-bulb temperature T (K) was obtained from the ASHRAE correlation (1):

$$\ln P_{sw} = C_8 / T + C_9 + C_{10}\,T + C_{11}\,T\,2 + C_{12}\,T\,3 + C_{13} \ln T \quad (1)$$

where the ASHRAE constants are $C_8 = -5.800\,2006 \times 10^3$, $C_9 = 1.394\,1499 \times 10^0$, $C_{10} = -4.864\,0239 \times 10^{-2}$, $C_{11} = -4.176\,4768 \times 10^{-5}$, $C_{12} = -1.445\,2093 \times 10^{-8}$ and $C_{13} = 6.545\,9673 \times 10^0$. The partial vapour pressure of the air sample at measured relative humidity RH was then computed from (2):

$$P_v = RH \times P_{sw}$$

The humidity ratio W (kg of water vapour per kg of dry air) followed from the psychrometric mass-ratio identity (3):

$$W = 0.622\,P_v / (P - P_v)$$

where P denotes the local barometric pressure. The specific enthalpy h of the moist-air sample (kJ/kg of dry air) and the specific volume v (m³/kg) were obtained from (4) and (5):

$$h = 1.006\,T + W\,(2501 + 1.86\,T)$$

$$v = R_a\,T / (P - P_v)$$

with $R_a = 287.055$ J kg^{-1} K^{-1} and T in kelvin. The air mass flow rate at the coil outlet was derived from the outlet volumetric flow Q and the local outlet density ρ = 1/v (6):

$$\dot{m}_a = Q_o / v_o$$

The sensible, latent and total cooling rates (Q_s, Q_l and Q_t) were evaluated from (7)–(9):

$$Q_s = \dot{m}_a\,c_{p,a}\,(T_{ai} - T_{ao})$$

$$Q_t = \dot{m}_a\,(h_i - h_o)$$

$$Q_l = Q_t - Q_s \quad (1)$$

The moisture removal rate (MRR, kg/h) and dehumidification effectiveness (ε_d) were defined as in (10) and (11):

ISSN 2250-3676 ijesatj@gmail.com https://www.ijesat.com/

International Journal of Engineering Science and Advanced Technology (IJESAT)
Vol 26 Issue 05, May 2026
Received: 19-03-2026 Accepted: 25-04-2026 Published: 02-05-2026

$$MRR = \dot{m}a\ (Wi - Wo) \times 3600 \quad (10)$$

$$\varepsilon d = (Wi - Wo) / (Wi - Weq) \quad (11)$$

where W_eq is the air humidity ratio in equilibrium with the local LD film at its bulk temperature and concentration, evaluated from the LiCl property correlations of Conde and tabulated by ASHRAE. The uncertainties in Q_s, Q_t and MRR, propagated from the instrument specifications of Table I using the Moffat method, were within ±6 %, ±8 % and ±9 % respectively of the reported values.

V. RESULTS AND DISCUSSION

A. Sample calculation

A representative test point taken in the LD-off mode with T_w = 17 °C is presented in detail to illustrate the data-reduction procedure. The recorded inputs are T_{ai} = 35.7 °C, RH_i = 36.4 %, T_{ao} = 28.3 °C and RH_o = 53.6 %. The wet-bulb temperature at the inlet evaluated iteratively from (1)–(4) is T_{wb} = 25.2 °C. The saturation vapour pressure at the outlet dry-bulb temperature, computed from (1), is ln(P_sw) = 8.13, giving P_sw = 3.403 kPa. The corresponding partial vapour pressure is P_v = 1.657 kPa. The humidity ratio at the outlet is W_o = 11.5 g/kg of dry air, the enthalpies are h_i = 67.3 kJ/kg and h_o = 52.7 kJ/kg, and the specific volume at the outlet is v_o = 0.862 m³/kg. The density of air at the outlet is ρ_o = 1.160 kg/m³. The outlet volumetric flow is Q_o = 0.126 m³/s, yielding an air mass flow rate of 0.146 kg/s. Substitution in (7) gives Q_s = 1.248 kW and substitution in (8) gives Q_t = 2.139 kW; the latent component from (9) is therefore Q_l = 0.891 kW. The corresponding MRR from (10) is 1.0 kg/h. These values anchor the consolidated test matrix reported next.

B. Consolidated test matrix

Table II summarises the principal measured and derived quantities for the four operating points (two water temperatures × two operating modes). The table follows the structure of the raw laboratory data sheet to preserve the original measurements without rounding.

TABLE II
COIL PERFORMANCE UNDER CHILLED-WATER-ONLY AND LD-INTEGRATED OPERATION AT TWO CHILLED-WATER INLET TEMPERATURES

Parameter	Unit	Water	Water	LD+Water	LD+Water
		T_n=17°C	T_n=22°C	T_n=17°C	T_n=22°C
ΔT_a	°C	6.7	3.7	7.4	3.2
Dew-point, inlet	°C	18.1	19.6	18.1	19.7
Wet-bulb, inlet	°C	25.2	25.3	25.2	25.3
LD average temp.	°C	—	—	—	—
$\dot{m}_a$	kg/s	0.2	0.2	0.2	0.2
Δh	kJ/kg	11.7	7.1	8.7	5.7
W_i (inlet)	g/kgda	13.4	14.7	13.4	14.8
W_o (outlet)	g/kgda	11.5	13.4	12.9	14.2
ΔW	g/kgda	1.9	1.3	0.4	0.6
Q_s (sensible)	kW	1.4	0.8	1.6	0.9
Q_t (total)	kW	2.5	1.5	1.9	1.2
Q_l (latent)	kW	1.1	0.7	0.3	0.3
MRR	kg/h	1.4	1.0	0.3	0.4

C. Coil baseline: chilled-water-only operation

With chilled water at 17 °C and no LD sprayed, the coil delivered a large air-temperature depression of 6.7 °C and a sizeable enthalpy drop of 11.7 kJ/kg. Because the coil surface temperature was below the local air dew point (18.1 °C), the coil operated as a wet cooling coil: the inlet humidity ratio of 13.4 g/kg dropped to 11.5 g/kg, corresponding to a ΔW of 1.9 g/kg and a moisture removal rate of 1.4 kg/h. The sensible cooling rate Q_s was 1.4 kW and the latent cooling rate Q_l was 1.1 kW, giving a total cooling rate Q_t of 2.5 kW and a sensible heat ratio (SHR) of 0.56. This baseline establishes the reference upper bound for the coil's capacity.

Raising the chilled-water inlet temperature to 22 °C—above the inlet dew point of 19.6 °C—suppresses condensation on the coil and reduces both ΔT_a and ΔW. The air-temperature depression falls to 3.7 °C, the enthalpy drop

2250-3676 ijesatj@gmail.com https://www.ijesat.com/

International Journal of Engineering Science and Advanced Technology (IJESAT)
Vol 26 Issue 05, May 2026
Received: 19-03-2026 Accepted: 25-04-2026 Published: 02-05-2026

falls to 7.1 kJ/kg, and the humidity ratio drop drops to 1.3 g/kg, principally attributable to small pockets of the coil surface that fall below the local dew point at fin contraction locations. The sensible and latent cooling rates are 0.8 and 0.7 kW, respectively, with a total cooling rate of 1.5 kW. This is in close agreement with the classical decoupling behaviour of VCR coils: once the surface rises above the dew point, latent handling collapses and the coil functions as a sensible-only element.

D. Effect of LD integration at T_n = 17 °C

When the LiCl spray was introduced onto the coil that had just been operating with T_w = 17 °C (Table II, column 5), two opposing effects were observed simultaneously. On one hand, the sensible cooling increased from 1.4 kW to 1.6 kW (a 14 % uplift) and the air-temperature depression increased from 6.7 °C to 7.4 °C; this is attributable to the additional sensible transfer associated with the falling film and the exothermic heat-of-absorption liberation that further preheats the LD but simultaneously raises the air-to-film temperature difference at the leading edge of the coil. On the other hand, the latent cooling collapsed from 1.1 kW to 0.3 kW and the MRR dropped from 1.4 kg/h to 0.3 kg/h. The net effect was a reduction of the total cooling rate from 2.5 kW to 1.9 kW (a 24 % penalty) and a shift of the SHR from 0.56 to 0.84.

Three mechanisms explain the observed latent-cooling penalty. (i) The aqueous LiCl film adds a new thermal resistance between the air stream and the chilled-water surface, raising the effective surface temperature above the dew point and suppressing condensation of water vapour out of the air. (ii) The large air-side mass flow rate (0.155 kg/s for a compact coil frontal area) translates into a short residence time per air parcel in the active contacting zone, so that mass-transfer equilibrium between the air and the LD film is not approached. (iii) The ambient LD was admitted at room temperature (around 30 °C at the pump outlet), so that the thermodynamic driving potential for moisture absorption—the difference between the water vapour pressure in the air and on the desiccant surface—was smaller than that between the air and a cold wet coil surface.

E. Effect of LD integration at T_n = 22 °C

At T_w = 22 °C—where the baseline coil cannot condense moisture out of the air—the LD integration delivered the qualitative benefit that an LD system is intended to provide: dehumidification above the air dew point. The LD-integrated run (Table II, column 6) produced a ΔW of 0.6 g/kg and an MRR of 0.4 kg/h, compared with 1.3 g/kg and 1.0 kg/h for the corresponding chilled-water-only baseline at 22 °C. While the absolute latent performance is still modest, the crucial observation is that dehumidification was obtained at a surface temperature that is 2.4 °C above the air dew point—a regime in which a conventional coil alone cannot dehumidify. The total cooling rate is 1.2 kW, again lower than the corresponding chilled-water-only baseline (1.5 kW) because of the thermal resistance effect described previously, but the SHR has shifted from 0.53 (coil-only) to 0.75 (LD-integrated), indicating that a portion of the capacity has been redirected from sensible to latent handling—consistent with the intent of a hybrid LDAC design.

F. Comparative analysis

The supplementary bar charts summarising the ΔW, latent cooling and total cooling (Fig. 4) for the chilled-water-only baseline at the two investigated water temperatures confirm the trend that lower chilled-water temperatures favour both sensible and latent performance. Quantitatively, dropping T_w from 22 °C to 17 °C lifts ΔW by 46 %, latent cooling by 57 % and total cooling by 67 %, which is a strong indication that the integrated hybrid performance is primarily controlled by the chilled-water temperature when LD integration is not yet optimised for wetting and residence time.

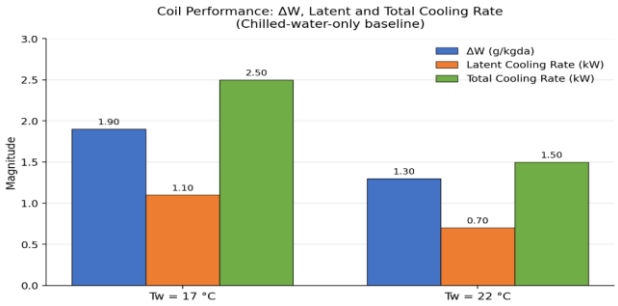

Fig. 4. Humidity ratio depression (ΔW, g/kgda), Latent cooling rate (kW) and Total cooling rate (kW) delivered by the coil in chilled-water-only operation at the two investigated chilled-water inlet temperatures.

The measured penalty associated with LD integration is consistent with the internal-cooling framework recently reviewed by Guan et al. [42] and quantitatively modelled by Luo et al. [44]: the driving potential for mass transfer scales with the vapour-pressure difference between the air and the desiccant surface, which in turn scales inversely with the film temperature. A chilled water temperature near the dew point, combined with a room-temperature LD inlet, yields a film temperature that is too close to the air dew point to provide a substantial driving potential. Pre-cooling of the LD prior to the spray, or a higher LD-to-air mass-flow ratio (the present tests operated near 0.15, compared with the 0.3–0.5 range recommended by Shukla and Modi [61] for falling-film devices), are expected to significantly improve both ΔW and the total cooling at matched SHR.

The results also suggest that the penalty in total cooling is partially a consequence of the coupling between sensible and latent handling in the integrated device. Once the LD is sprayed on the coil, the surface becomes warmer than the chilled-water return, which reduces the log-mean temperature difference on the chilled-water side (and hence the sensible duty available for the air stream), while the small MRR means that only a small share of the latent load is converted to an exothermic absorption contribution. This is the same trend

2250-3676 ijesatj@gmail.com https://www.ijesat.com/

identified by Zhang et al. [48] in the 4-NTU–Le formulation, and is a well-known optimisation frontier for internally-cooled LDAC devices.

VI. CONCLUSIONS AND FUTURE WORK

An instrumented experimental study of a vertically oriented finned-tube mini-channel heat exchanger used simultaneously as the evaporator of a VCR chiller and as the internally cooled contacting surface of a liquid-desiccant dehumidification loop has been reported. The coil was tested at two chilled-water inlet temperatures (17 °C, below the air dew point, and 22 °C, above the air dew point) in two operating modes (chilled-water-only baseline and chilled-water + aqueous LiCl spray). The principal conclusions are as follows.

First, the mini-channel coil alone delivered a peak total cooling rate of 2.5 kW at Tw = 17 °C, with sensible and latent components of 1.4 kW and 1.1 kW respectively and a moisture removal rate of 1.4 kg/h. The high compactness and surface-area-to-volume ratio of the mini-channel geometry translate directly into substantial cooling per unit coil volume, confirming the intrinsic thermal-hydraulic advantage of mini-channel surfaces.

Second, the integration of the LD spray at the same chilled-water inlet conditions produced a marginal increase in sensible cooling (1.4 kW → 1.6 kW) but a pronounced reduction in latent cooling (1.1 kW → 0.3 kW) and total cooling (2.5 kW → 1.9 kW). The penalty originated from the thermal resistance of the desiccant film, the short gas–liquid contact time at the tested face velocity and the elevated LD inlet temperature relative to the air dew point.

Third, at T_w = 22 °C—above the air dew point—the LD-integrated mode delivered measurable dehumidification (ΔW = 0.6 g/kg, MRR = 0.4 kg/h) where the coil-only baseline produced negligible latent handling. This confirms the fundamental advantage of hybrid LDAC operation: moisture removal is possible at coil surface temperatures above the air dew point, eliminating the overcooling-then-reheat penalty inherent to conventional VCR systems.

Fourth, the system is highly sensitive to the LD-to-air mass-flow ratio and to the LD inlet temperature. Operating at an LD-to-air mass ratio near 0.15 with room-temperature LD is insufficient to realise the full potential of the internally-cooled contactor. Pre-cool

ing of the LD (to obtain a lower film temperature and a larger driving vapour-pressure difference), increased LD mass flow rate, and improved surface wetting through hydrophilic coatings or distributor redesign are identified as the dominant levers for future performance improvement.

Future work will investigate: (i) the use of a dedicated LD pre-cooler that shares its rejection heat with the regenerator; (ii) variable-area distribution headers to improve film uniformity across the mini-channel fin surface; (iii) the replacement of aqueous LiCl by mixed LiCl–$CaCl_2$ solutions and by selected ionic liquids to lower regeneration temperature; and (iv) the coupling of the mini-channel coil with an indirect evaporative cooling post-stage to push the supply dry-bulb temperature closer to the ambient wet-bulb while maintaining the latent-handling duty inside the LD loop.

REFERENCES

[1] International Energy Agency, *The Future of Cooling: Opportunities for Energy-Efficient Air Conditioning*. Paris, France: IEA, 2018.

[2] X. Chen, S. Riffat, H. Bai, X. Zheng, and D. Reay, "Recent progress in liquid desiccant dehumidification and air-conditioning: A review," *Energy Built Environ.*, vol. 1, no. 2, pp. 106–130, Apr. 2020.

[3] H.-L. Park, S.-J. Lee, J.-H. Lee, and J.-W. Jeong, "A liquid desiccant-assisted free-cooling system for energy-efficient data centers in hot and humid climates," *Case Stud. Therm. Eng.*, vol. 52, art. 103683, Dec. 2023.

[4] N. Khosravi, D. Aydin, M. Karim Nejhad, and P. A. Dogramaci, "Comparative performance analysis of direct and desiccant assisted evaporative cooling systems using novel candidate materials," *Energy Convers. Manage.*, vol. 221, art. 113167, Oct. 2020.

[5] Z. Bai, A. Chinnappan, J. Deng, C.-M. Shu, E. R. Ghomi, S. Yao, X. Duan, B. Chinnappan, and S. Ramakrishna, "Recent progress in ionic liquids as desiccants for energy consumption in cooling applications," *J. Mol. Liq.*, vol. 383, art. 122033, Aug. 2023.

[6] H. Bai, J. Zhu, J. Chu, X. Chen, Y. Cui, and Y. Yan, "Influences of the mixed LiCl-$CaCl_2$ liquid desiccant solution on a membrane-based dehumidification system," *Energy Build.*, vol. 183, pp. 592–606, Jan. 2019.

[7] A. Das, R. S. Das, and K. Das, "Performance analysis of aqueous LiCl and $CaCl_2$ based falling film dehumidifier with surface modification," *Appl. Therm. Eng.*, vol. 200, art. 117704, Jan. 2022.

[8] K. Kumar, A. Singh, P. K. Chaurasiya, K. K. Pathak, and V. Pandey, "Progressive development in hybrid liquid desiccant-vapour compression cooling system: A review," *Sustain. Energy Technol. Assess.*, vol. 55, art. 102960, Feb. 2023.

[9] K. Qu, G. Barreto, M. Iten, Y. Wang, and S. Riffat, "Energy and thermal performance of optimised hollow fibre liquid desiccant cooling and dehumidification systems in Mediterranean regions," *Energy*, vol. 263, art. 125852, Jan. 2023.

[10] O. Allahham, K. Ghali, and N. Ghaddar, "Novel energy efficient integration of chimney ventilation, liquid desiccant dehumidification, and evaporative cooling for humid climates," *Energy Convers. Manage.*, vol. 308, art. 118383, May 2024.

[11] B. Guan, T. Zhang, J. Liu, X. Liu, and Y. Yin, "Review of internally cooled liquid desiccant air dehumidification: Materials, components, systems, and

performances," *Build. Environ.*, vol. 211, art. 108747, Mar. 2022.

[12] P. R. Naveen and A. Kolakoti, "A review of internal cooling strategies in liquid desiccant dehumidification and cooling systems," *Int. J. Thermofluids*, vol. 22, art. 100688, May 2024.

[13] Y. Zhang, H. Zhang, H. Yang, Y. Chen, and C. W. Leung, "Counter-crossflow indirect evaporative cooling-assisted liquid desiccant dehumidifier: Model development and parameter analysis," *Appl. Therm. Eng.*, vol. 217, art. 119231, Dec. 2022.

[14] W. Li and Y. Yao, "Performance analysis of different flow types of internally-cooled membrane-based liquid desiccant dehumidifiers," *Energy*, vol. 228, art. 120563, Aug. 2021.

[15] Y. Wang, B. Ruhani, M. A. Fazilati, S. M. Sajadi, A. Alizadeh, and D. Toghraie, "Experimental analysis of hollow fiber membrane dehumidifier system with SiO_2/$CaCl_2$ aqueous desiccant solution," *Energy Rep.*, vol. 7, pp. 2821–2835, Nov. 2021.

[16] N. M. Shah, J. R. Mehta, and S. Sharma, "Parametric investigations on a novel bubble column liquid desiccant dehumidifier with internal cooling," *Energy Built Environ.*, vol. 5, no. 2, pp. 316–329, Apr. 2024 (Available online Feb. 2023).

[17] S. G. Kandlikar, *Heat Transfer and Fluid Flow in Minichannels and Microchannels*, 2nd ed. Oxford, U.K.: Elsevier, 2014.

[18] T. Wen, H. Zhan, and D. Zhang, "Flow boiling heat transfer in mini channel with serrated fins: Experimental investigation and development of new correlation," *Int. J. Heat Mass Transf.*, vol. 134, pp. 45–58, May 2019.

[19] N. Tran and C.-C. Wang, "Optimization of the airside thermal performance of mini-channel-flat-tube radiators by using composite straight-and-louvered fins," *Int. J. Heat Mass Transf.*, vol. 160, art. 120163, Oct. 2020.

[20] J. Hipchen, R. D. Weed, M. Zhang, and D. Nasuta, "Simulation-based comparison of optimised AC coils using small-diameter copper and aluminium micro-channel tubes," in *Proc. Int. Refrig. Air Cond. Conf.*, 2012, Paper 1305.

[21] A. Arteconi, G. Giuliani, M. Tartuferi, and F. Polonara, "Characterization of a mini-channel heat exchanger for a heat pump system," *J. Phys., Conf. Ser.*, vol. 501, art. 012023, 2014.

[22] W. Indrawan, A. Lubis, Nasruddin, and M. I. Alhamid, "The experimental study of dehumidification and regeneration processes in a fin and tube liquid desiccant system," *Case Stud. Therm. Eng.*, vol. 39, art. 102440, Nov. 2022.

[23] S. Fang, Z. Xu, X. Zhou, H. Zhang, X. Zhi, L. Qiu, and K. Wang, "Cascade deep air dehumidification with integrated direct-contact cooling and liquid desiccant absorption," *Energy Convers. Manage.*, vol. 268, art. 115959, Sep. 2022.

[24] G. Zhang, J. Tan, J. Xie, B. Du, H. Liu, and J. Liu, "Experimental and 4 NTU-Le heat and mass transfer model theoretical analysis based on a novel internally cooled liquid desiccant dehumidifier," *Energy*, vol. 297, art. 131308, Jun. 2024.

[25] Y. Wang, T. Dong, W. Cao, P. Peng, and F. Jiang, "Experimental investigation of the laminar flow and heat transfer performance of a harmonica tube with or without mini-fins," *Appl. Therm. Eng.*, vol. 175, art. 115373, Jul. 2020.

[26] A. Vangeffelen, G. Buckinx, C. De Servi, M. R. Vetrano, and M. Baelmans, "Nusselt number for steady periodically developed heat transfer in micro- and mini-channels with arrays of offset strip fins subject to a uniform heat flux," *Int. J. Heat Mass Transf.*, vol. 195, art. 123145, Oct. 2022.

[27] T. Wen, H. Zhan, and D. Zhang, "Flow boiling heat transfer correlation for mini-channels with serrated fins," *Int. J. Heat Mass Transf.*, vol. 134, pp. 45–58, May 2019.

[28] J. Li, D. Zhang, Y. Wang, W. Chen, and G. Zhu, "Pressure drop of R134a in mini channels with micro pin fins during flow boiling," *Appl. Therm. Eng.*, vol. 217, art. 119195, Dec. 2022.

[29] A. Vaisi, K. Javaherdeh, and R. Moosavi, "Condensation heat transfer performance in multi-fluid compact heat exchangers with wavy and strip fins," *Int. J. Heat Mass Transf.*, vol. 182, art. 121968, Feb. 2022.

[30] S. W. Chang and Z. C. Chen, "Hydrothermal performance of turbulent channel flow enhanced by spirally finned tube bundle in pitching and rolling motions," *Therm. Sci. Eng. Prog.*, vol. 37, art. 101567, Jan. 2023.

[31] G. Zhu, T. Wen, and D. Zhang, "Machine learning based approach for the prediction of flow boiling/condensation heat transfer performance in mini channels with serrated fins," *Int. J. Heat Mass Transf.*, vol. 166, art. 120783, Feb. 2021.

[32] T. Wen, G. Zhu, and L. Lu, "Experimental and artificial neural network based study on the heat transfer and flow performance of ZnO-EG/water nanofluid in a mini-channel with serrated fins," *Int. J. Therm. Sci.*, vol. 170, art. 107149, Dec. 2021.

[33] T. Wen, L. Lu, H. Zhong, and B. Shen, "Thermal properties measurement and performance evaluation of water/ZnO nanofluid in a mini channel with offset fins," *Int. J. Heat Mass Transf.*, vol. 162, art. 120361, Dec. 2020.

[34] M. M. Ozturk, B. Doğan, and L. B. Erbay, "Performance analysis of a compact heat exchanger with offset strip fin by non-uniform uninterrupted fin length," *Appl. Therm. Eng.*, vol. 160, art. 113991, Sep. 2019.

[35] M. Bahiraei and A. Monavari, "Irreversibility characteristics of a mini shell and tube heat exchanger operating with a nanofluid considering effects of fins and nanoparticle shape," *Powder Technol.*, vol. 398, art. 117117, Jan. 2022.

[36] M. Venegas, S. Ghatos, M. de Vega, and N. García-Hernando, "Experimental evaluation of a new mini square channel air-cooled heat exchanger for an absorption chiller," *Int. J. Heat Mass Transf.*, vol. 195, art. 123186, Oct. 2022.

[37] H. Bai, J. Zhu, J. Chu, X. Chen, Y. Cui, and Y. Yan, "Influences of the mixed LiCl-$CaCl_2$ liquid desiccant solution on a membrane-based dehumidification system: Parametric analysis and mixing ratio selection," *Energy Build.*, vol. 183, pp. 592–606, Jan. 2019.

[38] A. Das, R. S. Das, and K. Das, "Performance analysis of aqueous LiCl and $CaCl_2$ based falling film dehumidifier with surface modification," *Appl. Therm. Eng.*, vol. 200, art. 117704, Jan. 2022.

[39] M. Ijas Ahmed and L. Gangadhara Kiran Kumar, "Dehumidification performance of liquid desiccant system with aqueous-$CaCl_2$ solution in a humid climatic condition," *Mater. Today, Proc.*, vol. 46, pp. 9656–9661, 2021.

[40] Z. Bai *et al.*, "Recent progress in ionic liquids as desiccants for energy consumption in cooling applications," *J. Mol. Liq.*, vol. 383, art. 122033, Aug. 2023.

[41] D. Wei, Q. Cui, E. Gao, P. Qi, and X. Zhang, "Study on the heat transfer characteristics of CO_2 and liquid desiccant $CaCl_2$ aqueous solution in the gas cooler and evaporator," *Int. J. Therm. Sci.*, vol. 197, art. 108830, Mar. 2024.

[42] B. Guan, T. Zhang, J. Liu, X. Liu, and Y. Yin, "Review of internally cooled liquid desiccant air dehumidification," *Build. Environ.*, vol. 211, art. 108747, Mar. 2022.

[43] P. R. Naveen and A. Kolakoti, "A review of internal cooling strategies in liquid desiccant dehumidification and cooling systems," *Int. J. Thermofluids*, vol. 22, art. 100688, May 2024.

[44] J. Luo, Q. Wang, Y. Zhang, and H. Yang, "A view on the performance comparison between adiabatic and internally-cooled dehumidification processes using liquid desiccant," *Desalination*, vol. 586, art. 117881, Oct. 2024.

[45] Y. Zhang, H. Zhang, H. Yang, Y. Chen, and C. W. Leung, "Counter-crossflow indirect evaporative cooling-assisted liquid desiccant dehumidifier," *Appl. Therm. Eng.*, vol. 217, art. 119231, Dec. 2022.

[46] Y. Zhang, H. Zhang, H. Yang, Y. Chen, and C. W. Leung, "Response surface modeling and optimization scheme of an internally cooled liquid desiccant air conditioning system," *J. Build. Eng.*, vol. 76, art. 107371, Oct. 2023.

[47] W. Li and Y. Yao, "Performance analysis of different flow types of internally-cooled membrane-based liquid desiccant dehumidifiers," *Energy*, vol. 228, art. 120563, Aug. 2021.

[48] G. Zhang *et al.*, "Experimental and 4 NTU-Le heat and mass transfer model theoretical analysis based on a novel internally cooled liquid desiccant dehumidifier," *Energy*, vol. 297, art. 131308, Jun. 2024.

[49] Y. Wang *et al.*, "Experimental analysis of hollow fiber membrane dehumidifier system with SiO_2/$CaCl_2$ aqueous desiccant solution," *Energy Rep.*, vol. 7, pp. 2821–2835, Nov. 2021.

[50] W. Indrawan, A. Lubis, Nasruddin, and M. I. Alhamid, "The experimental study of dehumidification and regeneration processes in a fin and tube liquid desiccant system," *Case Stud. Therm. Eng.*, vol. 39, art. 102440, Nov. 2022.

[51] N. M. Shah, J. R. Mehta, and S. Sharma, "Parametric investigations on a novel bubble column liquid desiccant dehumidifier with internal cooling," *Energy Built Environ.*, vol. 5, no. 2, pp. 316–329, 2024.

[52] P. Pasqualin and P. A. Davies, "Concept design of a greenhouse cooling system using multi-stage nanofiltration for liquid desiccant regeneration," *Appl. Therm. Eng.*, vol. 216, art. 119057, Nov. 2022.

[53] P. Pasqualin and P. A. Davies, "Dynamic simulation of a novel liquid desiccant air-conditioning system for greenhouse cooling and water recovery," *Appl. Therm. Eng.*, vol. 242, art. 122495, Apr. 2024.

[54] H.-L. Park, S.-J. Lee, J.-H. Lee, and J.-W. Jeong, "A liquid desiccant-assisted free-cooling system for energy-efficient data centers in hot and humid climates," *Case Stud. Therm. Eng.*, vol. 52, art. 103683, Dec. 2023.

[55] O. Allahham, K. Ghali, and N. Ghaddar, "Novel energy efficient integration of chimney ventilation, liquid desiccant dehumidification, and evaporative cooling for humid climates," *Energy Convers. Manage.*, vol. 308, art. 118383, May 2024.

[56] S. Huang and H. Fu, "A hybrid technology for enhancing VOC transfer in liquid desiccant dehumidifiers: Combining surfactant and internal cooling," *Appl. Therm. Eng.*, vol. 247, art. 123017, Jun. 2024.

[57] S. Huang, H. Fu, and L. Wen, "Performance enhancement analysis of a liquid desiccant dehumidifier with internal cooling for indoor benzene removal," *Appl. Therm. Eng.*, vol. 243, art. 122552, Apr. 2024.

[58] K. Kumar, A. Singh, P. K. Chaurasiya, K. K. Pathak, and V. Pandey, "Progressive development in hybrid liquid desiccant-vapour compression cooling system: A review," *Sustain. Energy Technol. Assess.*, vol. 55, art. 102960, Feb. 2023.

[59] X. Chen, S. Riffat, H. Bai, X. Zheng, and D. Reay, "Recent progress in liquid desiccant dehumidification and air-conditioning: A review," *Energy Built Environ.*, vol. 1, no. 2, pp. 106–130, Apr. 2020.

[60] Y. Zhang, J. Xiong, G. Mao, and J. Li, "Ideal mass transfer cycle and thermal performance optimization for liquid desiccant air conditioning system," *Results Phys.*, vol. 57, art. 107343, Feb. 2024.

[61] D. L. Shukla and K. V. Modi, "Influence of distinct input parameters on performance indices of dehumidifier, regenerator and on liquid desiccant-operated evaporative cooling system — A critical review," *Renew. Sustain. Energy Rev.*, vol. 168, art. 112834, Oct. 2022.

[62] K. Qu, G. Barreto, M. Iten, Y. Wang, and S. Riffat, "Energy and thermal performance of optimised hollow fibre liquid desiccant cooling and dehumidification systems in Mediterranean regions: Modelling, validation and case study," *Energy*, vol. 263, art. 125852, Jan. 2023.

[63] N. Khosravi, D. Aydin, M. Karim Nejhad, and P. A. Dogramaci, "Comparative performance analysis of direct and desiccant assisted evaporative cooling systems using novel candidate materials," *Energy Convers. Manage.*, vol. 221, art. 113167, Oct. 2020.

[64] S. Fang *et al.*, "Cascade deep air dehumidification with integrated direct-contact cooling and liquid desiccant absorption," *Energy Convers. Manage.*, vol. 268, art. 115959, Sep. 2022.